Turkish Computational and Theoretical Chemistry

Turkish Comp Theo Chem (TC&TC)

Volume (Issue): 9(1) – Year: 2025 – Pages: 1-18

e-ISSN: 2602-3237

https://doi.org/10.33435/tcandtc.1487560

Received: 22023 ***Accepted***: 05.06.2023 *Research Article*

A Computational Approach of Anti-diabetic Potential Evaluation of Flower and Seed of Nyctanthes arbor tristis Linn

Ram Lal Swagat Shrestha[a,b], Nirmal Parajuli[a], Prabhat Neupane[a], Sujan Dhital[a], Binita Maharjan[a,b], Timila Shrestha[a,b], Samjhana Bharati[a,b], Bishnu Prasad Marasini[c], Jhashanath Adhikari Subin[d, 1]

[a]*Department of Chemistry, Amrit Campus, Tribhuvan University, Lainchaur, Kathmandu 44600, Nepal*
[b]*Kathmandu Valley College, Syuchatar Bridge, Kalanki, Kathmandu 44600, Nepal*
[c]*Nepal Health Research Council, Ramshah Path, Kathmandu 44600, Nepal*
[d]*Bioinformatics and Cheminformatics Division, Scientific Research and Training Nepal P. Ltd., Bhaktapur 44800, Nepal*

Abstract: Exploring the medicinal significance of bioactive compounds through computational methods is an increasingly practiced approach in contemporary medicinal research. This study aims to assess the antidiabetic potential of compounds extracted from the plant *Nyctanthes arbor tristis* by evaluating their ability to inhibit the carbohydrate metabolic enzyme α-glucosidase. The research work was conducted through molecular docking calculation, molecular dynamics simulation (MDS), and ADMET prediction techniques. Among the compounds, arbortistoside-C (NAS03), and arbortristoside-D (NAS04) found in the seed of the plant were identified as hit inhibitors of the target protein with docking scores, -9.9 and -9.4 kcal/mol, respectively. The compounds showed a comparable docking score with the drug of diabetes acarbose (-8.6 kcal/mol). Geometrical parameters like radius of gyration, solvent accessibility surface, root mean square deviation, and root mean square fluctuation from MDS supported the stability of the protein-ligand complex. MMPBSA calculations demonstrated the stability and feasibility of the complex with binding free energy changes of -29.06±6.06 and -23.58±8.80 kcal/mol for compounds NAS03 and NAS04, respectively. The ADMET prediction suggested the drug-likeness of the compounds compared with that of the standard drugs. The results could be used in proposing the antidiabetic potential of the two compounds from the plant as ~~a~~ potential inhibitors of α-glucosidase enzyme. Further, *in vitro* and *in vivo* experiments on such compounds could be a more reliable path to validate the output of this computational research.

Keywords: Molecular docking, Glucosidase inhibitors, Molecular dynamics simulation, Binding free energy calculation, ADMET prediction

Graphical abstract:

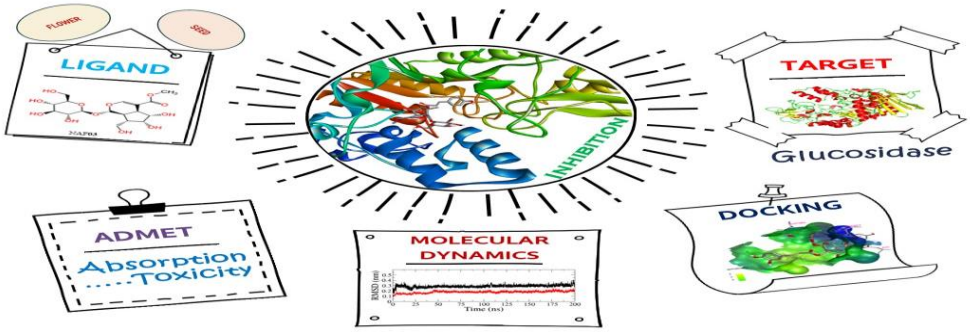

[1] Corresponding Authors

e-mail: subinadhikari2018@gmail.com

1. Introduction

Hyperglycemia is a chronic disease that is predominant in all age groups in the world. High blood sugar conditions which might be due to dysfunctional islets of Langerhans cells (pancreas), kidney, liver, skeletal muscle, and brush border (small intestine), cause well-known carbohydrate metabolic disorders, diabetes mellitus, or type II diabetes (T2D) [1]. It is mainly reported as an inborn (genetic) disease or caused by side effects of daily dietary consumption and lifestyle. The scientific control of T2D around the globe is a challenge and is a health burden [2].

Nyctanthes arbor tristis, also known as Parijat, is a reupdated medicinal plant, as reported by its various ethnomedicinal potentials in previous works [3]. The therapeutic spectrum as an antioxidant, antidiabetic, antineoplastic, and against other viral, bacterial, and chronic diseases signifies the medicinal aptitude of the plant [4-9]. This research work is focused on the exploration of the antidiabetic potential of the floral and seed parts of *N. arbor tristis* through computational virtual screening via molecular docking, molecular dynamics simulation (MDS), and pharmacokinetics prediction of the bioactive compounds found in this plant.

In silico method to evaluate the medicinal significance of a compound is a simple, automated, advanced, and comparatively low-cost approach [10]. Computer-based drug design enhances high throughput screening (HTS) by correlating experimental and computational results [11]. The evidence shows the understanding of the structure, working mechanism, and inhibition of carbohydrate metabolic enzymes (alpha-amylase, glucosidase, and other biocatalysts responsible for sugar catalysis) could be an important practice to minimize T2D [12,13]. Molecular docking calculation and molecular dynamics simulation (MDS) are the tools to interpret the effective interactions, and validate the stability of the complex between enzyme and compound in a virtual approach for the estimation of the activity of the compounds over specific enzymes at its catalytic site and to specify their possible impact on the enzyme [14]. The docking tool demonstrates the best binding orientation and calculates its affinity towards the catalytic amino acid residues at the active site pocket of the enzyme. The MDS interprets the stability of the docked complex with various geometric and thermodynamic parameters [15]. Root mean square deviation (RMSD), radius of gyration (R_g), solvent accessibility surface area (SASA), hydrogen bond count, and binding free energy change are the valuable components that could calculate the stability of the complexes in the form of numeral values using MDS trajectory.

ADMET prediction is a tool to predict the pharmacodynamics and pharmacokinetics of the selected compound [11]. It helps to interpret the activity of the bioactive compounds in absorption, distribution, metabolism, excretion, and toxicity phenomena in the human body in a normal physiological environment and temperature [16].

In this study previously reported compounds in *N. arbor tristis* were selected as the candidate for glucosidase enzyme inhibitors and further characterization through molecular dynamics simulation and their drug-likeness prediction were carried out.

2. Computational Method

2.1. Ligand Selection and Preparation

Phenolics, iridoids, and flavonoids found in the flower and seed of the plant were selected as the ligands for computation. The 3D structures of isolated compounds of the plant were downloaded from the PubChem database web server (https://pubchem.ncbi.nlm.nih.gov/) in sdf format [17]. The information of the ligand and standard reference drugs with respective PubChem CID is listed in Table 1.

The sdf format of the compound was converted into pdb format using the PyMol software and eventually changed into pdbqt with the help of the Autodock tools [18,19].

2.2. Target Protein Preparation and Molecular Docking Calculation

The target protein, alpha-glucosidase enzyme (PDB ID: **5ZCC**), an x-ray crystallographic structure of 1.704 angstrom resolution, was taken from the RCSB protein data bank (https://www.rcsb.org/) in pdb format [20]. Homology modeling of the target structure was done by using the Swiss-Model server (https://swissmodel.expasy.org/interactive) and a model having 99.64% sequence identity with a GMQE value of 0.99 was selected [21]. Using the PyMol software, water molecules, non-standard

residues attached to the enzyme, and co-crystallized ligand were removed. Polar hydrogen atoms addition, charge optimization by adding Kollman charge, grid box selection at the catalytic site of the target, and conversion of pdb format of protein into pdbqt for molecular docking calculation, were carried out with the help of AutoDock tools [18]. The grid box size and configurations during the docking are mentioned in Table 2.

The molecular docking calculation and binding affinity calculation were performed by AutoDock vina software with an energy range of 4 units, 20 modes, and an exhaustiveness of 64. A 0.5 **Å** RMSD between the cocrystal ligand and docked ligand, was obtained for the molecular docking protocol validation on the target protein since RMSD of less than 2 **Å** implies that the molecular docking algorithm is valid. The pictorial superposition of the ligands is presented in Figure 1. The Biovia Discovery Studio 2021 and PyMol software were used for visualization purposes [22].

Table 1: Selected compounds of the plant with PubChem CID

Plant Part	Ligands	Ligand ID	Molecular Formula	PubChem CID	Reference
Flower	Astragalin	NAF**01**	$C_{21}H_{20}O_{11}$	5282102	[23]
	Diethylene glycol Benzoate	NAF**02**	$C_{11}H_{14}O_4$	88603	[24]
	Nyctanthoside	NAF**03**	$C_{17}H_{26}O_{12}$	95224501	[23,25]
	2-phenyl gluco-β-pyranose	NAF**04**	$C_{14}H_{20}O_6$	11289099	[8]
	Rengyolone	NAF**05**	$C_8H_{10}O_3$	10725564	[8]
Seed	Arbortristoside-A	NAS**01**	$C_{27}H_{34}O_{13}$	6442162	[23,25]
	Arbortristoside-B	NAS**02**	$C_{26}H_{32}O_{15}$	6442163	[25]
	Arbortristoside-C	NAS**03**	$C_{26}H_{32}O_{13}$	23955893	[8,25]
	Arbortristoside-D	NAS**04**	$C_{26}H_{32}O_{15}$	14632886	[20]
	Arbortristoside-E	NAS**05**	$C_{27}H_{34}O_{13}$	14632884	[20]
	Nyctanthic acid	NAS**06**	$C_{30}H_{48}O_2$	12313631	[23]
Reference drugs	Acarbose	—	$C_{25}H_{43}NO_{18}$	41774	
	Miglitol	—	$C_8H_{17}NO_5$	441314	
	Voglibose	—	$C_{10}H_{21}NO_7$	444020	

Table 2: Grid box information used in target protein during molecular docking

Protein PDB	Grid box center			Grid box size (Å)			spacing
	x-axis	y-axis	z-axis	x-axis	y-axis	z-axis	0.375 (Å)
5ZCC	-0.655	53.715	72.724	30	30	30	

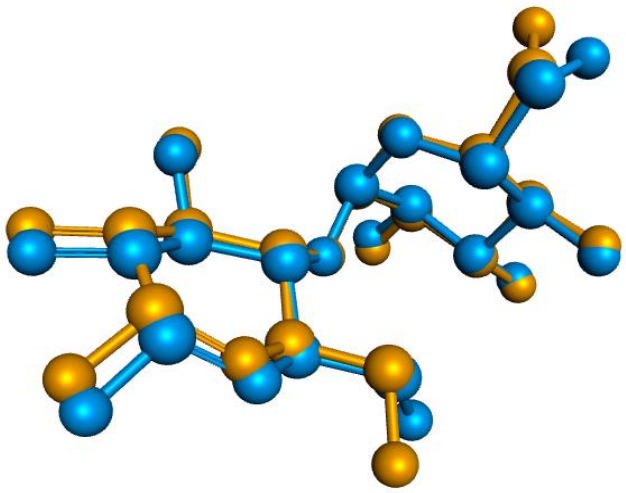

Figure 1: Superposition of co-crystallized (blue) and docked (orange) ligands (RMSD = 0.5 **Å**)

2.3 Molecular Dynamics Simulation (MDS)

Molecular dynamics simulation of the docked complex was performed as mentioned by Neupane et al., 2024 [26]. The GROMACS software (version 2021.2) was used to run MDS with the forcefield Charmm27 on the Swissparam server (https://www.swissparam.ch/) [27]. The equilibration of the system was done at 310 K in four steps with each of 1 ns and the volume temperature equilibration (NVT) and pressure-temperature equilibration (NPT) (2 steps for each) were carried out consecutively for the equilibration of the system. Different geometric parameters (R_g, SASA, RMSD, RMSF, and hydrogen bond count), and thermodynamic parameters (binding free energy change) calculations were carried out.

2.4. Free Energy Changes Calculation

The binding free energy change ($\mathbf{\Delta G_{BFE}}$) of the protein-ligand complex from the equilibrated part of the MDS trajectory was estimated by the MMPBSA method [28]. The spontaneity of the biochemical reaction in the system was calculated in terms of free energy change. The relation **(1)** was used to assess the energy change,

$$\mathbf{\Delta G_{BFE}} = \mathbf{G_{R\text{-}L\ complex}} - \mathbf{G_R} - \mathbf{G_L} \qquad (1)$$

$\mathbf{G_{R\text{-}L\ complex}}$ free energy of receptor-ligand complex, $\mathbf{G_R}$= free energy of receptor, and $\mathbf{G_L}$= free energy of ligand

Gmx-MMPBSA module considered gas phase molecular mechanics, internal energy, electrostatic solvation energy, van der Waals energy, and polar and non-polar contributors to the system during free energy change calculation [29]. Utilizing the free energy change, the binding constant was calculated [30].

2.5. ADMET Prediction

Pharmacokinetics and pharmacodynamics prediction of the ligands and reference drugs were carried out using the admetSAR (http://lmmd.ecust.edu.cn/admetsar2/) webserver [31]. The parameters (absorption, distribution, metabolism, excretion, and toxicity), and their endpoints were evaluated in terms of probability values.

2.6. Resources

Molecular docking calculations, data interpretation, and visualization were done using computer Windows 11 (8GB RAM, 8core CPU processor). Molecular dynamics simulations and binding free energy calculations were performed on Ubuntu 20.04.06 LTS operating system of 12th generation Intel processor with 24 cores and utilized an NVIDIA GPU accelerator.

3. Result and Discussion

3.1. Best poses of ligand

The docking of ligands at the orthosteric site of the enzyme could be the potential inhibitory or stimulatory process which depends on enzyme specificity [32]. The inhibition of the alpha-glucosidase could be a top-notch method to prevent the rapid degradation of post-prandial carbohydrates which increase the blood sugar level in the bloodstream [33-34]. Table 3 shows comprehensive information on the adduct including docking scores and types of interactions (ligand-protein and protein reference drug) with respective bond lengths, and the figurative 2D and 3D interactions of the protein-ligand complex are presented in Figure 3 including the hydrophobic surface on the protein. Among the selected ligands, NAS03, NAS04, NAS05, and NAS06 were found to bind most strongly with α-glucosidase enzyme (5ZCC) with docking scores, of -9.9, -9.4, -9.1, and -9.0 kcal/mol, respectively. The compounds were able to score better than the native ligand on redocking (-8.6 kcal/mol) and the reference drugs, voglibose, acarbose, and miglitol (-6.0, -8.6, and -5.4 kcal/mol, respectively). NAS03 interacted through H-bonding with amino acid residues THR409, TRP288, HIS103, ARG411, ASP60, and HIS103 with reasonable bond distance and bond angle. A quite smaller bond angle of ARG411 and HIS103 might be due to the choice of the rigid docking feature of auto dock vina. Similarly, in NAS04-5ZCC complex, residues ASP327, ASP382, and SER145 made hydrogen bonding by interacting with considerable H-bond angle and bond distance (Figure 4). The stability of both complexes was verified by MDS later on. MDS assesses the parameters to evaluate the stability and proper interactions between ligand interactive sites and protein binding site residues [35]. The binding

affinities (among hit candidates, native ligands, and reference drugs), and the comparative interaction analysis pointed to the excellent binding potential of candidates to the glucosidase which might eventually result in a good inhibitory capacity of the ligand to the enzyme.

The amino acid residues, ASP199, GLN256, ARG411, ASN258, HIS203, ASP327, and SER145 were found to bind with reference drug molecules and native ligands by hydrogen bonding with reasonable bond distance (<3 Å) [36]. Additionally, ASP199, ILE143, THR409, ASN258, ASP382, GLY384, HIS103, ASP388, and HIS326 were other residues that formed hydrogen bonds with selected ligands, drugs, and native ligand.

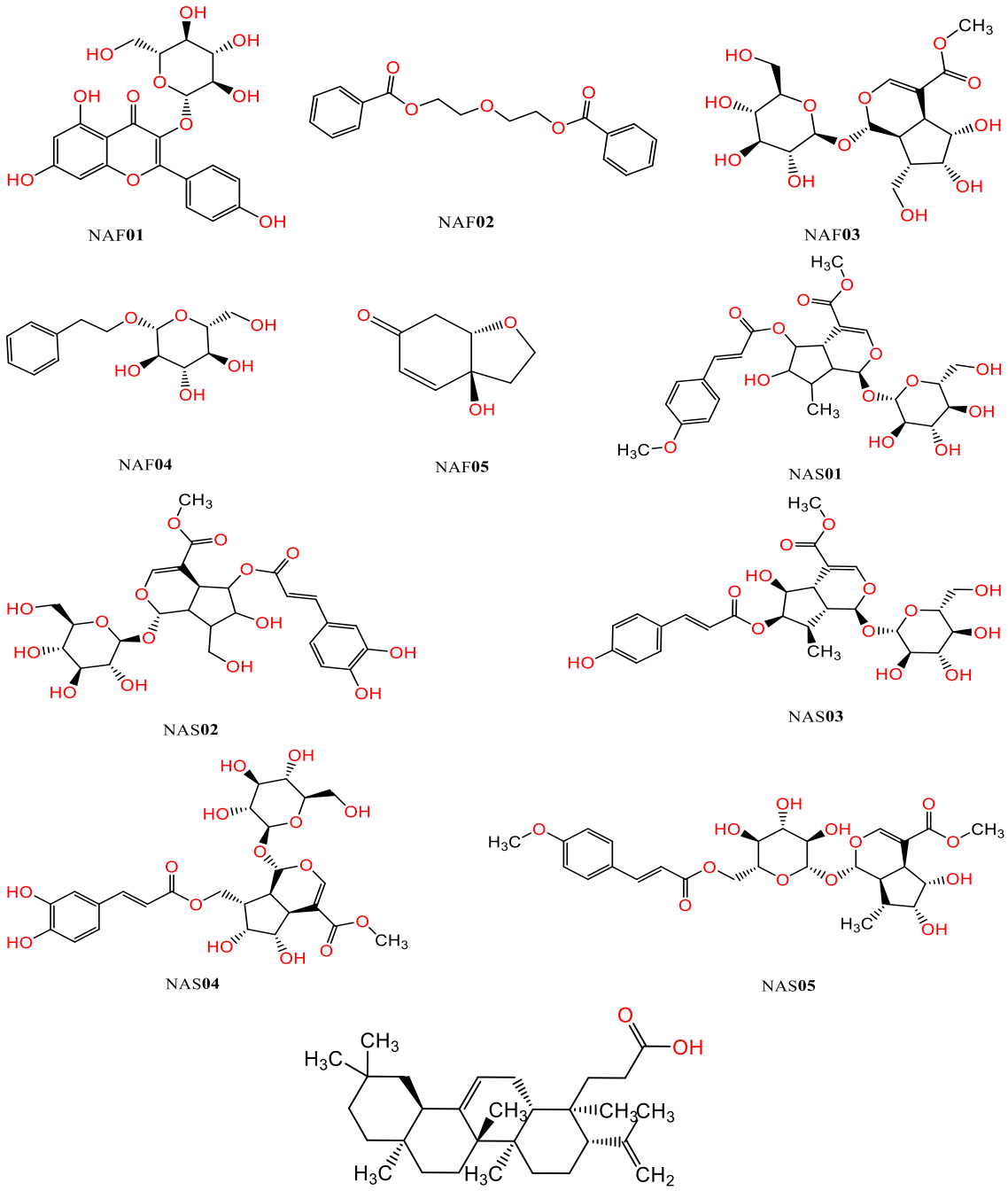

Figure 2: Molecular structures of selected compounds from the plant

Table 3: Ligand protein interaction of docked adduct with docking scores containing interaction distance

Ligand ID	Docking score (kcal/mol)	Type of interaction in ligand-protein complexes with bond length (Å)		
		H-bond	Hydrophobic interactions	Other interactions
NAF**01**	-8.6	ASN258 (2.83), TRP288 (2.27, 3.01)	ILE143 (5.47, 4.90), ASP327 (4.83)	PHE225, GLN256, PHE163, GYL286, **ARG411**, THR409
NAF**02**	-7.1	**GLN256** (2.29), ASP382 (2.07), GLY384 (3.53)	ASP327 (4.73), PHE163 (4.41), ALA200 (4.94)	ILE143, PHE144, HIS163, MET380
NAF**03**	-8.2	**GLN256** (2.74, 2.19), THE409 (2.78), **ARG411** (2.80), GLY384 (3.78)	MET385 (3.98)	ALA200, ASP327, GLN328, GLY382
NAF**04**	-7.5	**ASP327** (2.29), **ARG411** (2.84, 2.62)	PHE163 (4.04), ALA200 (4.83)	ASP60, HIS103, ILE143, GLN256, GLN328, MET385, ASP382
NAF**05**	-7.0	**ASP199** (2.06), **GLN256** (3.03, 2.02), **ARG411** (2.27), GLN167 (2.51), HIS103 (2.49)	PHE163 (5.15)	ARG197, ALA200, TYR63, ASP60, PHE144, ASP227, HIS320
NAS**01**	-8.1	HIS203 (2.47), ASN (1.98, 3.71), PHE (2.02, 2.24)	ASP327 (4.35), HIS326 (5.09), ALA200 (5.04), TYR63 (3.56), PHE225 (4.98),	ASP199, ILE143, ARG415, ASP60, PHE163, GLY259, MET229, **ARG411**
NAS**02**	-8.2	**ASP327** (2.54), GLN265 (2.35), **ASN258** (2.21), SER145 (2.34)	ILE143 (5.35)	SER142, PHE163, ALA200, PHE225, **ARG411**
NAS**03**	-9.9	ASP60 (2.10), HIS103 (2.60), ILE143 (2.34), **GLN256** (3.04), **ARG411** (2.96), TRP288 (2.59), THR409 (2.11), ASP388 (2.39)	PHE163 (3.96), ALA200 (4.91), ILE143 (4.70), TRP288 (5.06)	TYR63, PHE144, **ASP199**, GLY286, GLN328, MET385, ASP382, GLN167, PHE225
NAS**04**	-9.4	**ASP327** (2.54), ASP382 (2.10), SER145 (2.45), **ASP199** (3.14)	TRY63 (3.94), ILE143 (5.44)	ARG197, PHE163, SER142, GLN384, ARG411
NAS**05**	-9.1	HIS302 (2.68), **GLN256** (2.46), ASP382 (2.45), **ASP199** (3.44), **ASP327** (3.60)	TR63 (3.95), PHE225 (5.07), ILE143 (4.08), PHE282 (5.16)	ALA200, PHE163, TRP288, MET385, GLY384, **ARG411**
NAS**06**	-9.0	THR409 (2.03), **ARG411** (2.41)	ILE143 (5.05), PHE282 (4.45), ALA200 (4.86), HIS326 (5.28)	PHE144, ASP60, PHE225, GLN256, **ASP199**, SAP327, GLN328
Acarbose	-8.6	**ASP199** (2.74, 2.67), SER145 (2.29), ILE 143 (2.69), **GLN256** (2.15), **ASP327** (2.16), ASP 382 (2.54)	–	ARG197, ALA200, HIS103, PHE163, HIS203, ASP60, TYR63, HIS326, MET385, GLN328
Maglitol	-5.4	HIS203 (1.98), **GLN256** (1.99), ASN258 (2.38, 2.13), **ARG411** (2.50)	–	PHE163, ALA200, ASP327
Voglibose	-6.0	**ARG411** (2.50), **GLN256** (1.99), HIS203 (1.98), **ASN258** (2.13, 2.38)	–	ASP327, ALA200, GLN328, PHE163
Native ligand	-8.6	**GLN256** (2.14, 2.47, 2.90), ASP60 (2.52, 2.88), GLN167 (2.39), HIS103 (2.51), ASN258 (2.08, 2.53), HIS326 (2.49, 2.15), **ARG411** (2.52)	–	ARG197, PHE163, **ASP199**, HIS203, ARG 415

3D (a) *NAS03* **2D**

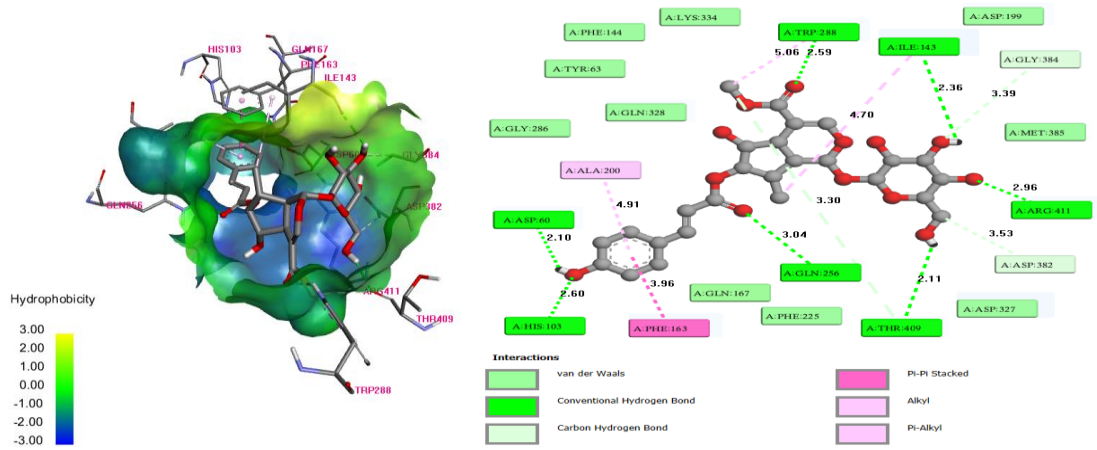

3D (b) *NAS04* **2D**

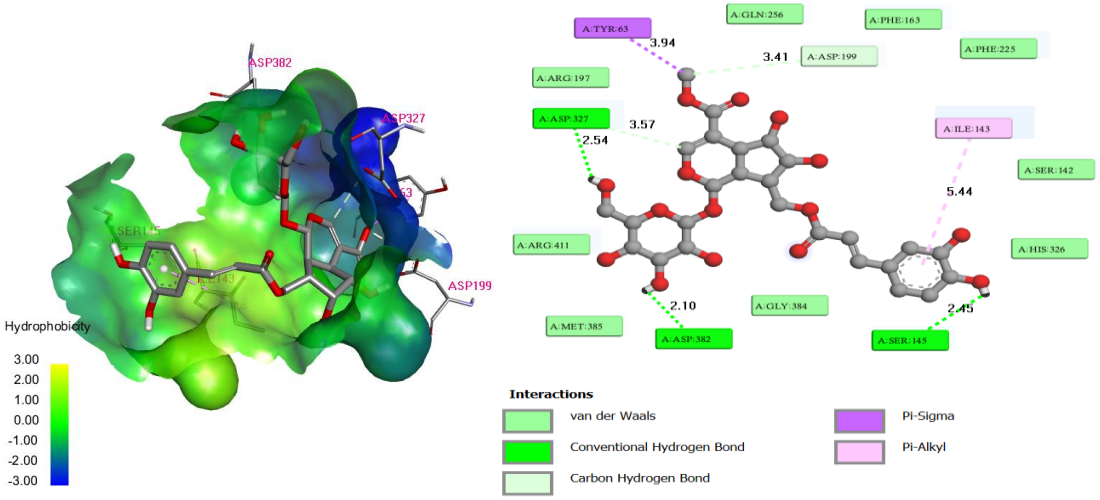

3D (d) ***Native*** **2D**

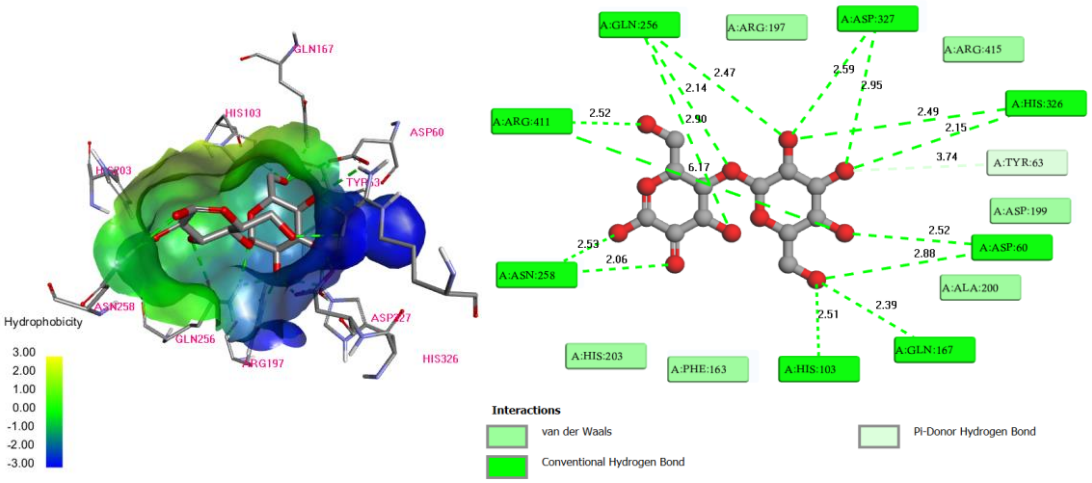

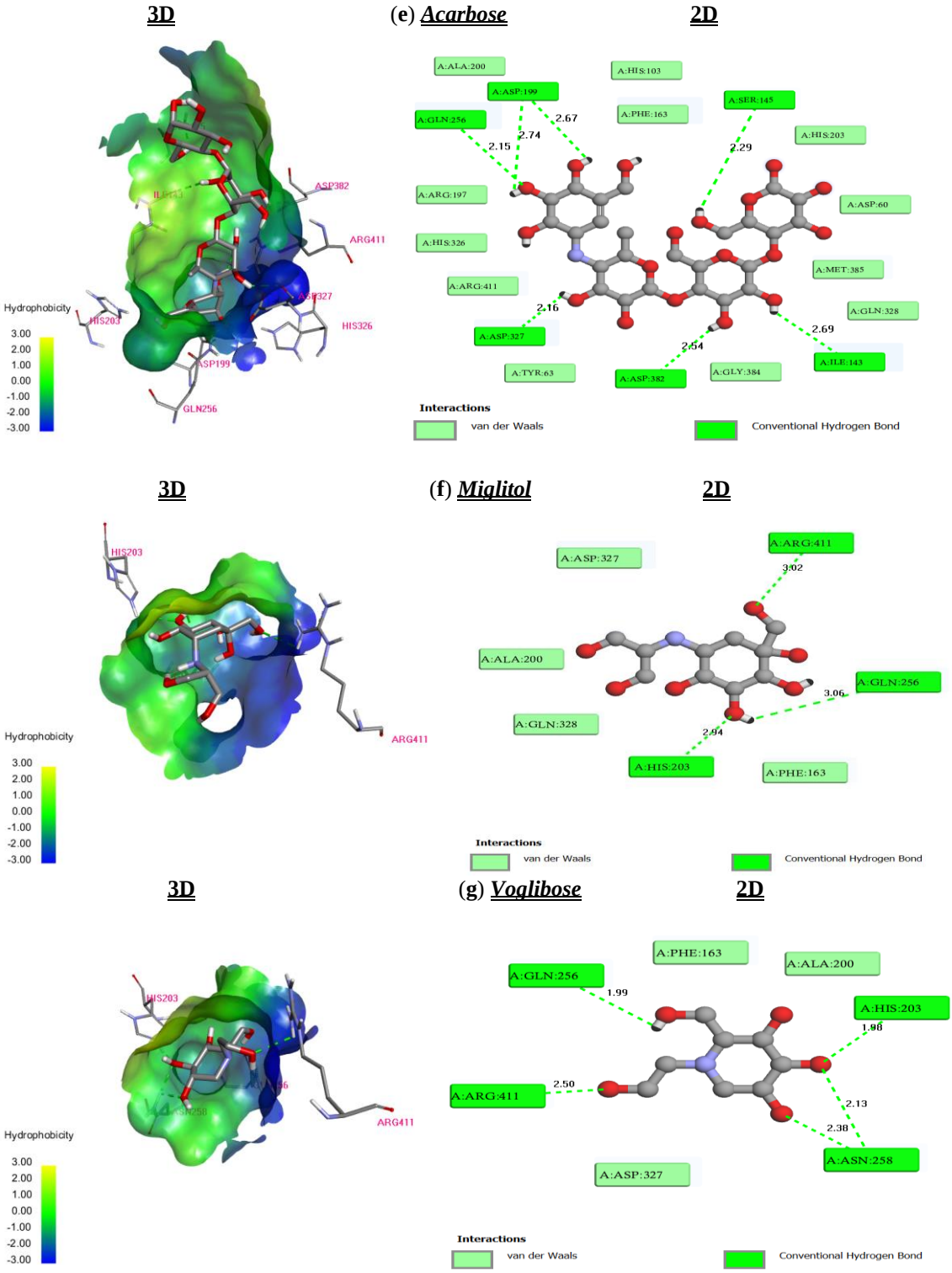

Figure 3: The 3D and 2D interactive presentation of the protein-selected ligand complex (**a** and **b**), protein-native ligand (**d**), and protein-drugs complex (**e-g**) with hydrophobicity on the surface of protein and bond length, where red, blue, grey, and black elemental representations in the 2D figure are for oxygen, nitrogen, carbon, and donor hydrogen, respectively.

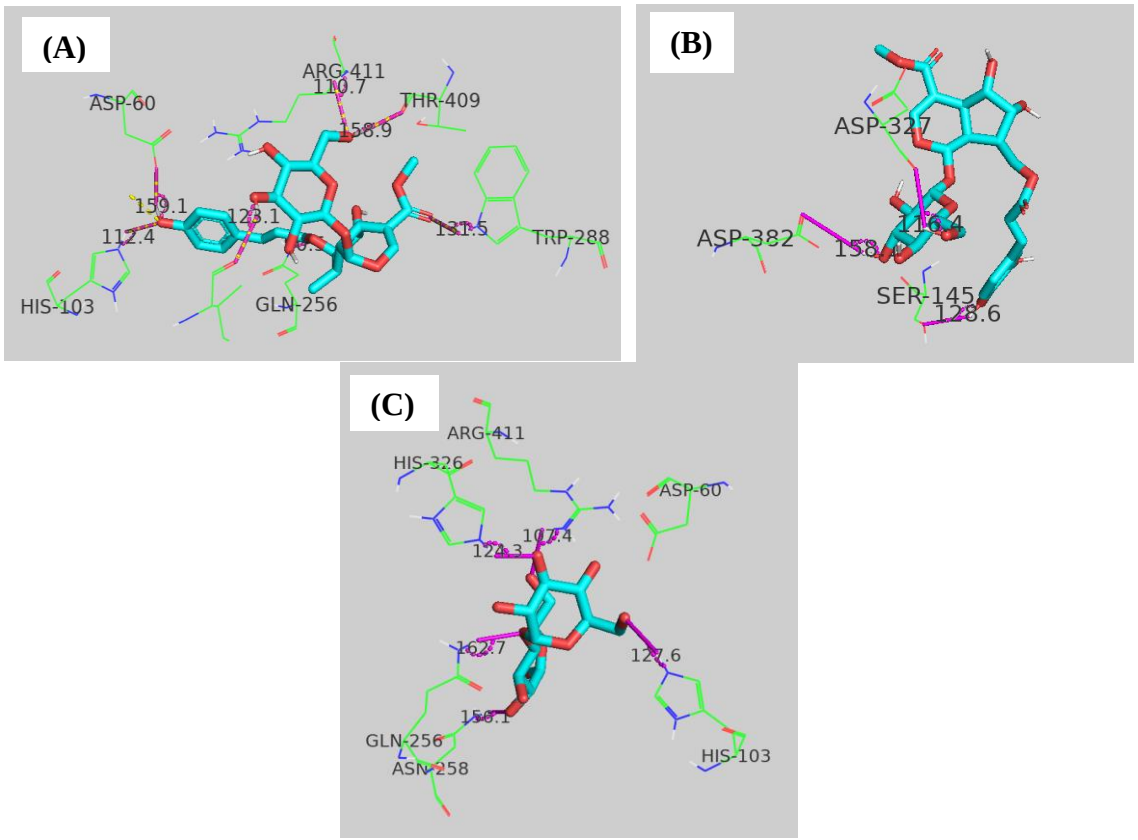

Figure 4: 3D interactions of the amino acid residues with a ligand containing H-bond angle in complexes (A) NAS**03**-5ZCC (B) NAS**04**-5ZCC and (C) Native-5ZCC

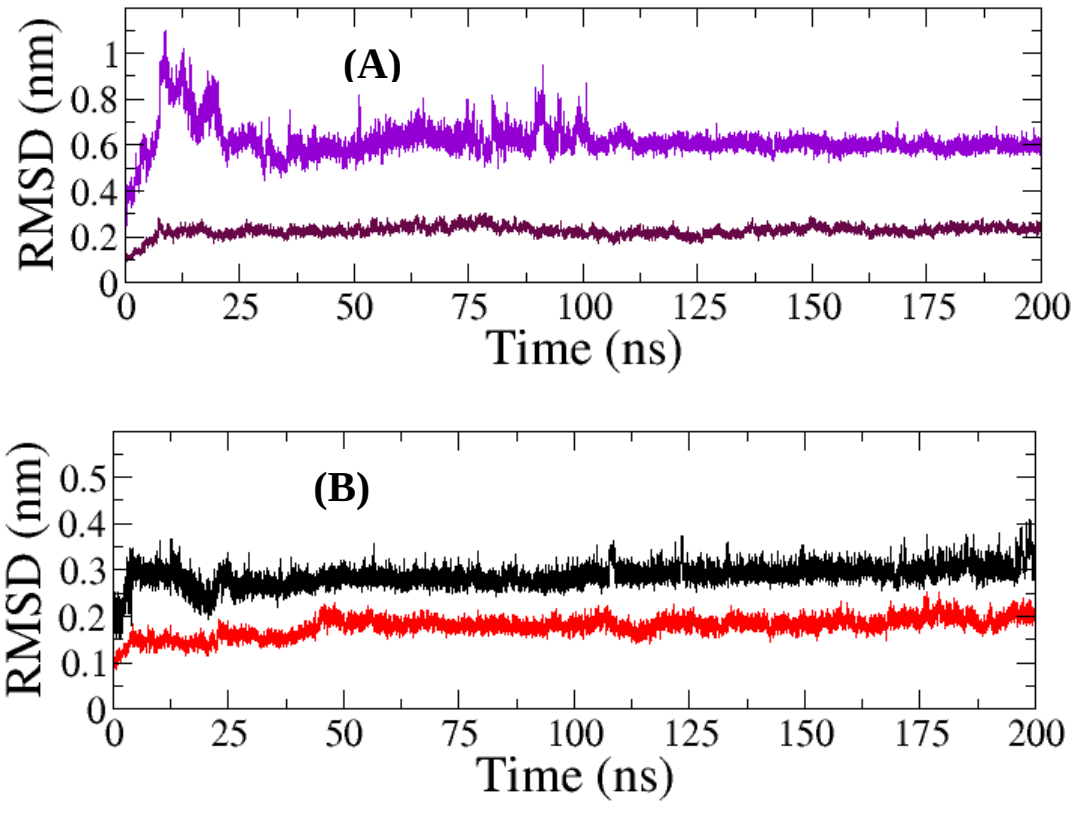

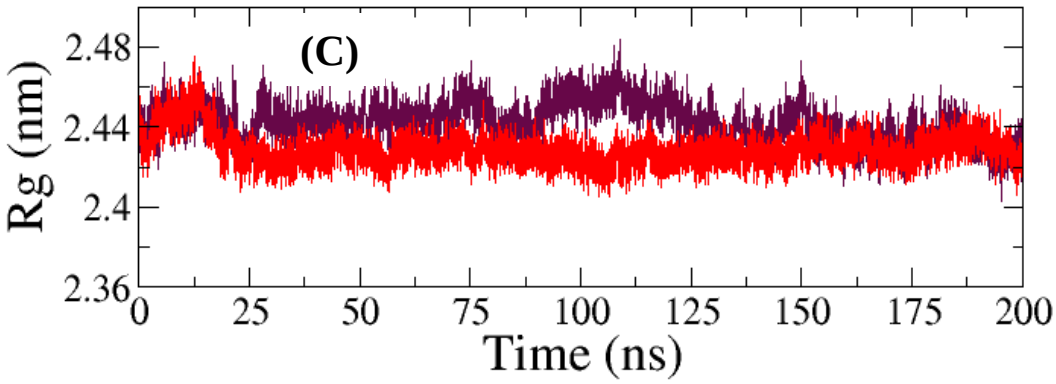

Figure 5: Root mean square deviation of (A) ligand *NAS**03*** (violet) and protein backbone (maroon), (B) ligand *NAS**04*** (black) and protein (red) both with respect to the protein backbone, and (C) radius of gyration of protein of *NAS**03**-5ZCC adduct (maroon), and NAS**04**-5ZCC adduct (red)*

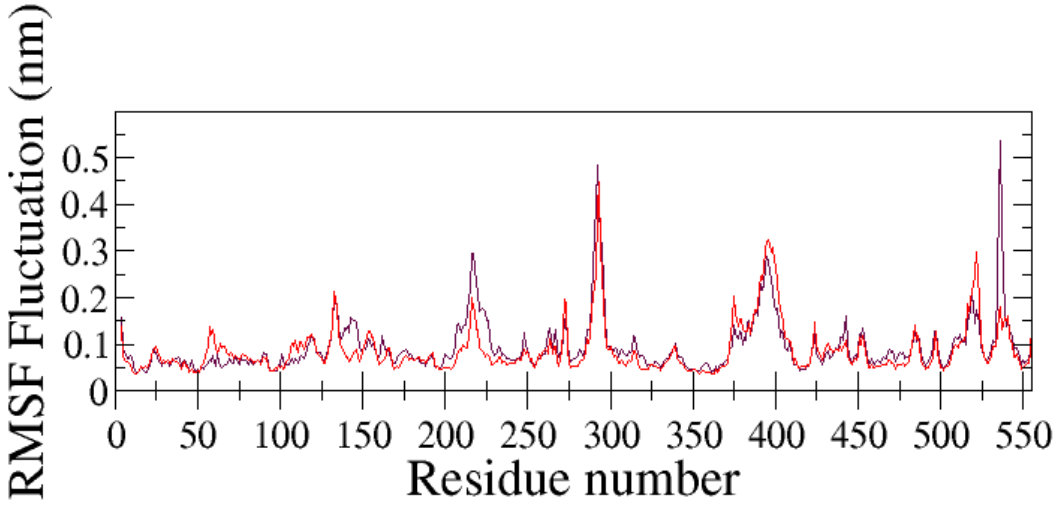

Figure 6: Root mean square fluctuation of protein backbone on the formation of a complex with *NAS**03*** (maroon) and *NAS**04*** (red)

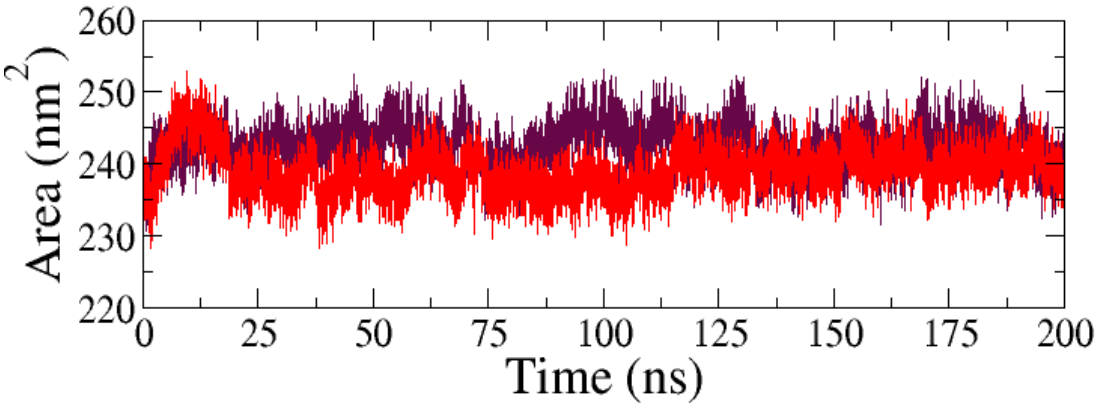

Figure** 7:* Solvent accessibility surface area changes with time of protein structure on complex formation with ligand *NAS**03 (maroon), *and NAS**04*** **(**red**)**

The hydrophobic interactions (Pi-Pi stacked, alkyl, Pi-alkyl, Pi-sigma, Pi-Pi T-shaped) were found to be predominant to the residues, ILE143, ASP327, PHE163, ALA200, MET385, HIS326, PHE225,

TYR63, and HIS326 [37]. Similarly, in the hit candidates, NAS (03-06), most of the active site residues formed hydrogen bonds (ASP327, ARG411, GLN256, ASP199) with bond distances less than 3 Å. So, the results portrayed a good binding orientation, position, and affinity of the ligands to the enzyme, and also the bond distance and bond angle portrayed a suitable docking pose and H-bond strength in the adduct at the enzyme pocket. Figure 4 illustrates the H-bond angle between donor-hydrogen-acceptor in protein-ligand interactions in complex formation with target found in some key and native ligands.**3.2. Geometrical Stability of Complexes**

The MDS provides the assessment of the stability of the adduct from molecular docking output. The parameters below were evaluated using statistical information from molecular dynamics simulation of the complexes.

3.2.1. Root mean square deviation (RMSD) and radius of gyration (R_g)

RMSD calculation of the simulated complex assesses the change in the position of the protein backbone and ligand from the original coordinates of the protein backbone with time [38]. Figure 5 shows the relative deviation of the protein backbone and ligand relative to the protein backbone. Among all complexes, *NAS**03**-5ZCC* and *NAS**04**-5ZCC* showed a stable trajectory for the period of 200 ns. For both complexes, the geometry of the receptor was found to be stable and equilibrated at RMSD 0.2 nm, meanwhile, ligand *NAS**03*** depicted the stable trajectory at about 0.6 nm after an initial 25 ns of equilibration (Figure 5A). Ligand ***NAS04-5ZCC*** was found to be stable throughout the simulation at an RMSD of 0.3 nm (Figure 4B). Relatively, the RMSD and trajectory followed by the complexes on simulation suggested the more stable complex formation by ligand *NAS**03*** with enzyme than that of the ligand *NAS**04*** with the target.

The radius of gyration gives the information of root mean square deviation of the atoms of protein from the centroid of it during simulation. The relative change in compactness and conformation of the protein structure after complex formation might be one of the crucial parameters to explain the stability of the complex [39]. Here, the protein structure in the *NAS**03**-5ZCC* complex and *NAS**04**-5ZCC* complex showed comparatively similar changes in R_g (at about 2.43 nm) on simulation (Figure 5C). The small fluctuations at about 15 ns and 100 ns might be due to the equilibration of the ligand on the binding pocket at the best pose and a slight change in the orientation of the ligands

3.2.2. Root Mean Square Fluctuation (RMSF)

RMSF assesses the deviation of the amino acid residues from their mean position at different regions of the protein backbone during MDS. The degree of fluctuation of the residue may decide the integrity of the protein backbone in adduct i.e., higher fluctuation in residue makes the complex less stable [15]. Figure 6 shows the RMS fluctuation profiles of the protein backbones after complex formation. In the *NAS**03**-5ZCC* complex, the backbone showed higher fluctuation (maroon), than in complex *NAS**04**-5ZCC* (red). The relatively higher fluctuation at some residue numbers, *ca.* 160, 225, 290, 390, 520, and 540 might be due to the absence of interactions (lower number of H-bonding and hydrophobic interactions), unfavorable interaction, or the presence of fluctuating loops and helix of the secondary structure of the protein.

3.2.3. Solvent Accessible Surface Area (SASA)

SASA is a useful geometric parameter to evaluate the interactive surface of protein to the solvent and the environment. It determines the nature of interactions in proteins and their stability in particular environments [40]. Figure 7 shows the different stages of SASA during MDS of the protein surface in the formation of the complex with ligands (NAS03 (maroon) and NAS04 (red)). The SASA for both complexes was found to be ca. 240 nm2. The lower fluctuation of the trajectory for SASA showed the stable nature of the adduct with a fixed exposed surface area (minimal fluctuations) of the protein to the solvent after adduct formation for 200 ns.

3.2.4. Hydrogen Bond Count

Hydrogen bonding is the strongest non-covalent interaction found in the hydrophilic surface of the receptor with the ligand. The hydrogen bond count accounts for other geometric parameters that depend on the proper orientation and interaction of the ligand in the binding site of the protein [41]. In this study, both ligands (*NAS**03*** and *NAS**04***) interacted with a significant number of hydrogen bonds (2 to 9) in the catalytic site of the protein during MDS (Figure 8). The ligand *NAS**03*** formed up to 7 hydrogen bonds whereas, the ligand *NAS**04***

formed mostly 8 hydrogen bonds overall in the adduct, which might play a vital role in the formation of stable adducts and help to support the other geometric parameters evaluating the stability of the complexes.

3.2.5. Free Energy Change in Complex Formation

Binding free energy change (ΔG_{BFE}) is a parameter to measure the spontaneity of the biochemical reaction at the body temperature [29]. Negative free energy change indicates the spontaneous behavior of the reaction or complex formation by comparing the energy change between reactants (protein and ligand) and products (complex) (equation 1). Table 4 indicates the degree of spontaneity in terms of free energy of the complex formation with two different ligands with the receptor.

Among the complexes, NAS03-5ZCC adduct carried a higher negative free energy change (-29.06±6.06 kcal/mol) than that of NAS04-5ZCC adduct (-23.58±8.80 kcal/mol). Even though free energy change calculations of both complexes was comparatively similar, the result showed a higher feasibility of complex formation with ligand NAS03 than with ligand NAS04 since more negative ΔGBFE on a specific reaction makes the product (complex) more spontaneous and stable thermodynamically. So, it could be said that the complex NAS03-5ZCC was more stable than that of NAS04-5ZCC thermodynamically concerning ΔGBFE.

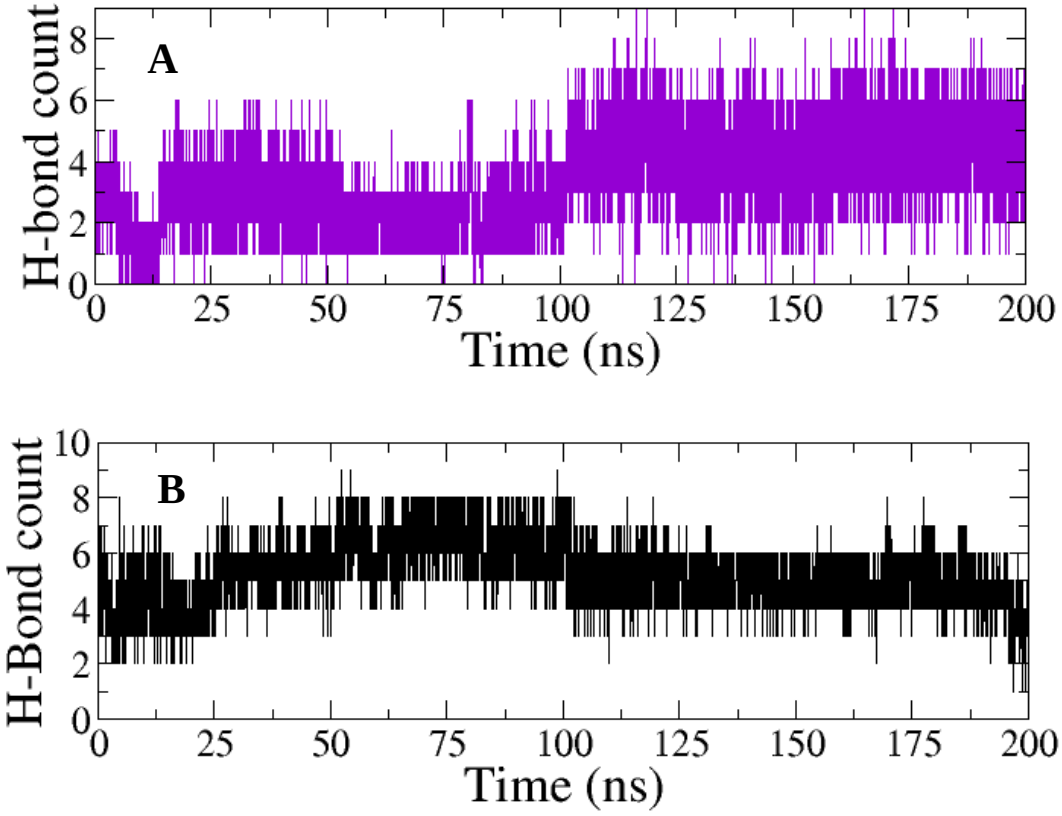

Figure 8: Hydrogen bond count in the complexes of protein with ligand *(A) NAS**03*** and *(B) NAS**04***

Table 4: Binding free energy change in complex formation with different ligands with receptors

Thermodynamic components	Free energy change in complexes (kcal/mol)	
	*NAS**03**-5ZCC*	*NAS**04**-5ZCC*
$\Delta E_{VDWAALS}$	-50.61±3.63	-48.20±4.42
ΔE_{EL}	-59.49±10.65	-68.88±14.13
ΔE_{PB}	86.73±8.29	99.23±8.57
ΔE_{MPOLAR}	-5.69±0.16	-5.73±0.17

ΔG_{SOL}	81.03±8.25	93.50±8.49
ΔG_{GAS}	-110.10±11.38	-117.08±12.18
ΔG_{BFE}	-29.06±6.06	-23.58±8.80
K_b	3.32×10^{-21}	5.62×10^{-17}

Note, ΔG_{BFE} = Binding Free Energy change, **ΔE_{GAS}** =Energy change in the gas phase, **ΔE_{ELE}** = Electrostatic energy, **ΔV_{DWAALS}** = van der Waal energy, **ΔG_{SOL}** = Electrostatic solvation energy, and **ΔG_{PB}** = Polar contributions in the solute-solvent system, **K_b**= Binding constant

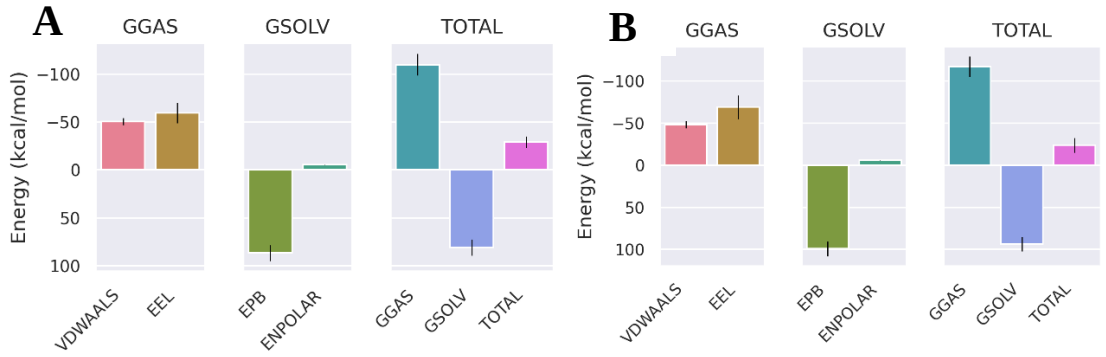

Figure 9: Different thermodynamic components and their contributions in free energy change of complexes (A) *NAS**03**-5ZCC* and (B) *NAS**04**-5ZCC*

Table 5: Comparative physiochemical properties of selected ligands with reference drugs in different aspects

Properties	Hit candidates and reference drugs				
	NAS**03**	NAS**04**	Acarbose	Miglitol	Voglibose
Molecular Weight	552.53	584.53	645.61	207.23	267.28
AlogP	-1.21	-2.53	-8.56	-3.26	-4.49
H-Bond Donor	6	8	14	5	8
H-Bond Acceptor	13	15	19	6	8
Rotatable Bonds	7	8	9	3	5

Figure 9 illustrates the considered thermodynamic energy parameters to calculate binding free energy change in adducts. The component ΔEPB was found disruptive although all other components were found associative in spontaneity evaluation.

3.3. ADMET prediction

The pharmacokinetic tendency of the selected candidates (compounds that were found stable through MDS) was virtually predicted using server-based admetSAR 2.0. Different structural configurations, molecular weights, hydrophobicity, and dimensions of the compounds on hydrogen bonding were estimated (Table 5). The hit ligands were of comparatively higher molecular weight (molecular weight>500 g/mol), than the active inhibitors of the glucosidase enzyme (miglitol, and voglibose), and were found similar to that of the drug acarbose. Additionally, the ligands were observed to be more hydrophilic than the standard drugs, as evidenced by their AlogP values.

Numbers of hydrogen bond donor and hydrogen bond acceptor and rotatable bonds on the ligands were found to be lower than acarbose and comparable to other drugs. The comparative properties of the ligands with the drugs are demonstrated in Table 5.

In this study, various parameters were considered for ADMET prediction as mentioned in Table 6. The different biophysical and biochemical endpoints in terms of the probability of active (+) and passive (-) values were estimated. Comparative activity of the ligands with standard drugs in terms of probability was calculated as mentioned in Table 6.

The selected ligands (*NAS**03*** and *NAS**04***) were found to be absorbable (+) in the human intestine though drugs were predicted to show low

absorbance in the intestinal cells. They showed the least absorption probability on the Caco-2 cell line and blood-brain barrier as shown by drugs. Both the ligands and drugs showed a low probability of human oral bioavailability except miglitol. Almost all the absorption parameters of the ligands were found comparable to the standard drugs.

On the major distributive and metabolic parameters, OATP1B1 enzyme inhibition (+), MATE1 inhibition (-), OCT2 inhibition (-), and P-glycoprotein inhibition (-), the ligands showed well-supported predictions, which were as predicted for drugs through the organic cationic and anionic absorption, toxin efflux, cellular excretion, and elimination. The positive inclination of the candidates towards the standard drugs supported their pharmacoactive nature. On the substrates, CYP3A4, CYP2D6, CYP2C19, and CYP1A2, ligands were predicted to follow a positive metabolic pathway as followed by acarbose and miglitol while ligands showed opposite result (+) on CYP2C8 inhibition than drugs which might point the inhibiting nature of the candidates to the activity of the enzyme cytochrome P450 2C8. CYP inhibitory promiscuity identified that all ligands and drugs might not interfere with the activity of the cytochrome P450 (CYP) enzyme which is crucial to check the alternation of the activity of multidrug target.

No ligands were found to have any carcinogenicity (binary or trinary) or mutagenetic phenomena. They pointed towards a negative probability of eye and skin irritation. The compounds did not have any hepatotoxic character though acarbose and voglibose might be toxic on prediction. They were found non-toxic to the respiratory tract although drugs were respiratory toxic and both compounds were found as toxic as drugs on reproductive, mitochondrial, and nephrotoxicity. Similarly, the crustacea aquatic toxicity and fish aquatic toxicity of the ligands were found to be negative (-) as of the drugs. Both the compounds and miglitol comprised class (III) on acute oral toxicity which might suggest the toxic nature of the ligands than drugs acarbose and voglibose. The predictions were similar (+) for both ligands as for the drug acarbose on estrogen receptor binding, thyroid receptor binding, and glucocorticoid receptor binding.

Table 6: ADMET prediction of selected ligands in various parameters compared with standard drugs

ADMET Parameters	Hit candidates and reference drugs									
	NAS**03**		NAS**04**		**Acarbose**		**Miglitol**		**Voglibose**	
	value	Prob.	value	Prob.	value	Prob.	value	Prob.	value	Prob.
Human Intestinal Absorption	+	0.656	+	0.625	-	0.965	-	0.659	-	0.587
Caco-2	-	0.890	-	0.905	-	0.895	-	0.866	-	0.916
Blood-Brain Barrier	-	0.650	-	0.650	-	0.800	-	0.700	-	0.725
Human oral bioavailability	-	0.871	-	0.828	-	0.900	+	0.971	-	0.857
OATP1B1 inhibitor	+	0.721	+	0.793	+	0.848	+	0.964	+	0.960
MATE1 inhibitor	-	0.940	-	0.840	-	1.000	-	0.980	-	1.000
OCT2 inhibitor	-	0.940	-	0.825	-	0.950	-	0.750	-	0.900
P-glycoprotein inhibitor	-	0.631	-	0.666	-	0.581	-	0.978	-	0.949
CYP3A4 substrate	+	0.631	+	0.655	+	0.592	-	0.594	-	0.566
CYP2D6 substrate	-	0.878	+	0.868	-	0.806	+	0.454	+	0.404
CYP2C19 inhibition	-	0.787	-	0.657	-	0.839	-	0.967	-	0.928
CYP1A2 inhibition	-	0.876	-	0.821	-	0.879	-	0.927	-	0.885
CYP2C8 inhibition	+	0.734	+	0.775	-	0.678	-	0.990	-	0.971
CYP inhibitory promiscuity	-	0.651	-	0.625	-	0.716	-	0.996	-	0.973
Carcinogenicity (binary)	-	1.000	-	1.000	-	0.980	-	0.950	-	0.870
Carcinogenicity (trinary)	*	0.648	*	0.643	*	0.640	*	0.661	*	0.717
Eye irritation	-	0.943	-	0.926	-	0.942	-	0.799	-	0.954
Skin irritation	-	0.784	-	0.802	-	0.821	-	0.905	-	0.758
Ames mutagenesis	-	0.583	-	0.523	-	0.530	-	0.520	-	0.910
Hepatotoxicity	-	0.825	-	0.800	+	0.912	-	0.630	+	0.950

skin sensitization	-	0.843	-	0.807	-	0.874	-	0.881	-	0.839
Respiratory toxicity	-	0.511	-	0.500	+	0.633	+	0.566	+	0.533
Reproductive toxicity	+	0.866	+	0.877	+	0.800	+	0.666	+	0.688
Mitochondrial toxicity	+	0.662	+	0.662	+	0.750	+	0.912	+	0.725
Nephrotoxicity	+	0.483	-	0.606	-	0.844	-	0.832	+	0.471
Acute Oral Toxicity (c)	III	0.536	III	0.546	IV	0.616	III	0.608	IV	0.626
Estrogen receptor binding	+	0.764	+	0.829	+	0.661	-	0.909	-	0.585
Androgen receptor binding	+	0.578	+	0.631	+	0.598	-	0.852	-	0.762
Thyroid receptor binding	+	0.564	+	0.533	-	0.500	-	0.784	-	0.517
Glucocorticoid receptor binding	+	0.628	+	0.546	-	0.525	-	0.720	-	0.595
PPAR gamma	+	0.746	+	0.704	+	0.585	-	0.909	-	0.677
Crustacea aquatic toxicity	-	0.680	-	0.710	-	0.620	-	0.920	-	0.690
Fish aquatic toxicity	+	0.832	-	0.818	-	0.816	-	0.988	-	0.941
Biodegradation	-	0.700	-	0.750	-	0.825	-	0.600	-	0.725

*Non-required

The comparative ADMET prediction of the hit candidates with drugs supported their pharmacokinetic efficiency. The affinity and bioactivity of the selected ligands towards the various enzymes responsible for the absorption, distribution, metabolism, and excretion of bioactive compounds without interrupting the normal functioning in comparison to the standard drugs support the drug-likeness properties.

This study demonstrated two compounds (*NAS**03*** and *NAS**04***) as hit candidates for effective binding with the glucosidase enzyme. Both compounds were of class Phyto-iridoids containing bulky hydrophobic benzene rings and an alkyl chain on their structure. Relative structural study of the hit candidates with the reference drugs suggests that the functional structure increment in the hydrophobic region of the ligands, either by substituted hydroxyl group, hetero element, heterocyclic ring, or other glycosides, would enhance the H-bond donor-acceptor ratio [42]. The changes would increase the probability of effective binding pose and orientation exhibiting a larger number of H-bonds with higher binding affinity and negative free energy change. The modification of the structures could result in the formation of a more stable complex with the glucosidase enzyme and could amplify as a lead inhibitor from hit. Using substructures of the hit compound helps in pharmacophore modeling.

The molecular docking, MDS and ADMET analysis of the hit compounds taken from previous literature on plant *N. arbor tristis* suggested the potential binding capability of the compounds to the glucosidase enzyme and their comparative drug-likeness to the standard drugs. Mainly, compounds found in the seed of the plant were found to have the best binding affinity to the target protein as suggested by evaluating the docking and the molecular simulation parameters of the complexes. A good binding capacity at the orthosteric site and stability of the complex on simulation with negative binding free energy might lead to a good inhibitory potential of the ligand to the hydrolase catalytic enzyme to regulate the release of monosaccharides in blood vessels which could be used as an enzyme inhibitor (glucosidase inhibitor) to treat the T2D. Based on the binding affinity, stability of the simulated complexes, binding free energy changes, and pharmacokinetics of the ligands, two of them (*NAS**03*** and *NAS**04***) were suggested to be potential glucosidase inhibitors found in the seed of the plant.

4. Conclusions

The α-glucosidase enzyme inhibition potential screening of the compounds found in *N. arbor tristis* was performed through molecular docking calculation and molecular dynamics simulation to evaluate the antidiabetic efficiency. Two iridoids reported in the seed of the plant, namely, arbortristoside-C (*NAS**03***) and Arbortristoside-D (*NAS**04***), were found to show the best binding affinity with the glucosidase enzyme and were able to preserve the position and pose in the complex. The ligands established good thermodynamic stability in complex formation with the enzyme. The drug-likeness of ligands from comparative ADMET prediction with standard drugs suggested a good pharmacokinetic property of the compounds. The result of this study proposed a good inhibitory potential of the compounds (*NAS**03*** and *NAS**04***) on the glucosidase enzyme which might be a potential

drug candidate to treat hyperglycemia. This research could help in approaching the antidiabetic drug design from the plant *N. arbor tristis* . Exploration of wide classes of phytochemicals found in other endemic species could enhance the scope of drug discovery utilizing natural products. The computational method evaluates an initial hypothesis regarding the pharmacological potential of compounds using virtual screening. Consensus docking calculations would help to validate and optimize the hit candidate through a computer-based technique further. The *in vitro*, and *in vivo* experimental interpretation and correlation of the hit compounds would be the future recommendation to interpret the lead candidate and its optimization.

References

[1] S. Chatterjee, K. Khunti, M. J. Davies. Type 2 diabetes, The Lancet. 389 (2017) 2239–2251.

[2] M. McGill, L. Blonde, J. C. N. Chan, K. Khunti, F. J. Lavalle, C. J. Bailey. The interdisciplinary team in type 2 diabetes management: Challenges and best practice solutions from real-world scenariosJ. Clin. Transl. Endocrinol. 7 (2017) 21–27

[3] P. K. Jain, A. Pandey. The wonder of Ayurvedic medicine-*Nyctanthes arbortristis*, Int. J. Herb. Med. 9 (2016) 9–17.

[4] M. Haque, N. Sultana, S. Abedin, N. Hossain, S. Kabir. Fatty acid analysis, cytotoxicity, antimicrobial and antioxidant activities of different extracts of the flowers of *Nyctanthes arbor-tristis* L., Bangladesh J. Sci. Ind. Res. 55 (2020) 207–214.

[5] K. Priya, D. Ganjewala, Antibacterial Activities and Phytochemical Analysis of Different Plant Parts of *Nyctanthes arbor tristis* (Linn.), Res. J. Phytochem. 1 (2007) 61–67.

[6] A. K. Singh, A. Kumar. Medicinal value of the leaves of *Nyctanthes arbor tristis* : A review, J. Med. Plants Stud. 10 (2022) 205–207.

[7] S. Pundir, G. Kumar Gautam, S. Zaidi. A Review on Pharmacological Activity of Nyctanthes *arbor tristis* , Res. J. Pharmacogn. Phytochem. 14 (2022) 69–72.

[8] N. K. S. M. Dewi, N. Fakhrudin, S. Wahyuono. A comprehensive review on the phytoconstituents and biological activities of *Nyctanthes arbor tristis* L., J. Appl. Pharm. Sci., 12 (2022) 9–17.

[9] T. Sana, S. Qayyum, A. Jabeen, B. S. Siddiqui, S. Begum, R. A. Siddiqui, T. B. Hadda. Isolation and characterization of anti-inflammatory and anti-proliferative compound, for B-cell Non-Hodgkin lymphoma, from *Nyctanthes arbor tristis Linn*., J. Ethnopharmacol. 293 (2022)

[10] G. C. Terstappen, A. Reggiani. In silico research in drug discovery, Trends Pharmaco. Sci. 22 (2001.

[11] S. J. Y. Macalino, V. Gosu, S. Hong, S. Choi. Role of computer-aided drug design in modern drug discovery, Arch. Pharm. Res. 38 (2015) 9.

[12] S. Basnet, M. P. Ghimire, T. R. Lamichhane, R. Adhikari, A. Adhikari. Identification of potential human pancreatic α-amylase inhibitors from natural products by molecular docking, MM/GBSA calculations, MD simulations, and ADMET analysis, PLoS One. 18 (2023) 01–13.

[13] J. Yi, T. Zhao, Y. Zhang, Y. Tan, X. Han, Y. Tang, G. Chen Isolated compounds from *Dracaena angustifolia* Roxb and acarbose synergistically/additively inhibit α-glucosidase and α-amylase: an in vitro study, BMC Complement. Med. Ther. 22 (2022) 1–12.

[14] X. Du, Y. Li, Y. L. Xia, S. M. Ai, J. Liang, P. Sang, X. L. Ji, S. Q. Liu. Insights into protein–ligand interactions: Mechanisms, models, and methods, Int. J. Mole. Sci. 17 (2016).

[15] L. Martínez. Automatic identification of mobile and rigid substructures in molecular dynamics simulations and fractional structural fluctuation analysis, PLoS One. 10 (2015).

[16] M. W. El-Saadi, T. Williams-Hart, B. A. Salvatore, E. Mahdavian. Use of in-silico assays to characterize the ADMET profile and identify potential therapeutic targets of fusarochromanone, a novel anti-cancer agent, Silico Pharmacol. 3 (2015).

[17] S. Kim, J. Chen, T. Cheng, A. Gindulyte, J. He, S. He, Q. Li, B. A. Shoemaker, P. A. Thiessen, B. Yu, L. Zaslavsky, J. Zhang, E. E. Bolton. PubChem 2023 update, 51 (2022) 1373–1380.

[18] O. Trott, A. J. Olson. AutoDock Vina: Improving the speed and accuracy of docking with a new scoring function, efficient optimization, and multithreading, J. Comput. Chem. 2009. https://doi.org/10.1002/jcc.21334

[19] S. Yuan, H. C. S. Chan, Z. Hu. Using PyMOL as a platform for computational drug design, Comput. Mol. Sci. 7 (2017).

[20] H. M. Berman, J. Westbrook, Z. Feng, G. Gilliland, T. N. Bhat, H. Weissig, I. N. Shindyalov, P. E. Bourne. The Protein Data Bank, (2000).

[21] A. Waterhouse, M. Bertoni, S. Bienert, G. Studer, G. Tauriello, R. Gumienny, F. T. Heer, T. A. P. De Beer, C. Rempfer, L. Bordoli, R. Lepore, T. Schwede. SWISS-MODEL: Homology modelling of protein structures and complexes, Nucleic Acids Res. 46 (2018) W296–W303, doi: 10.1093/nar/gky427.

[22] S. Shaweta, S. Akhil, and G. Utsav, Molecular Docking studies on the Anti-fungal activity of Allium sativum (Garlic) against Mucormycosis (black fungus) by BIOVIA discovery studio visualizer 21.1.0.0, Ann. Antivirals Antiretrovir. (2021) 028–032, doi: 10.17352/aaa.000013.

[23] J. Agrawal, A. *Pal. Nyctanthes arbor tristis* Linn - A critical ethnopharmacological review, J. Ethnopharmaco. 146 (2013) 645–658.

[24] M. M. Rahman, S. K. Roy, M. Husain, M. Shahjahan. Chemical constituents of essential oil of petals and corolla tubes of *Nyctanthes arbor tristis* linn flower, J. Essent. Oil-Bearing Plants. 14 (2011) 717–721.

[25] R. Chakraborty, S. Datta(De). A Brief Overview on the Health Benefits of *Nyctanthes arbor tristis Linn*.-A Wonder of Mother Nature, Indo Glob. J. Pharm. Sci. 12 (2022) 197–204.

[26] P. Neupane, J. Adhikari Subin, R. Adhikari. Assessment of iridoids and their similar structures as antineoplastic drugs by in silico approach. J. Biomol. Struct. Dyn. (2024) 1–16.

[27] V. Zoete, M. A. Cuendet, A. Grosdidier, O. Michielin. SwissParam: A fast force field generation tool for small organic molecules, J. Comput. Chem. 32 (2011) 2359–2368.

[28] A. V. Onufriev, D. A. Case. Generalized Born Implicit Solvent Models for Biomolecules. 2019.

[29] E. Wang, H. Sun, J. Wang, Z. Wang, H. Liu, J. Z. H. Zhang, T. Hou. End-Point Binding Free Energy Calculation with MM/PBSA and MM/GBSA: Strategies and Applications in Drug Design, Chemical Reviews. 119 (2019) 9478–9508.

[30] A. A. El-Bindary, A. F. Shoair, A. Z. El-Sonbati, M. A. Diab, E. E. Abdo. Geometrical structure, molecular docking and potentiometric studies of Schiff base ligand, J Mol Liq, 212 (2015) 576–584.

[31] F. Cheng, W. Li, Y. Zhou, J. Shen, Z. Wu, G. Liu, P. W Lee, Y. Tang. AdmetSAR: A comprehensive source and free tool for assessment of chemical ADMET properties, J. Chem. Inf. Model. 52 (2012) 3099–3105.

[32] I. A. Guedes, C. S. de Magalhães, and L. E. Dardenne, Receptor-ligand molecular docking, Biophys. Rev. 6(2014) 75–87.

[33] N. Cele, P. Awolade, P. Seboletswe, K. Olofinsan, M. S. Islam, P. Singh. α-Glucosidase and α-Amylase Inhibitory Potentials of Quinoline–1,3,4-oxadiazole Conjugates Bearing 1,2,3-Triazole with Antioxidant Activity, Kinetic Studies, and Computational Validation, Pharmaceuticals. 15 2022.

[34] R. L. S. Shrestha, R. Panta, B. Maharjan, T. Shrestha, S. Bharati, S. Dhital et al. Molecular docking and ADMET prediction of compounds from Piper longum L. Detected by GC-MS analysis in diabetes management. Mor. J. Chem. 12(2024) 776-798. https://doi.org/10.48317/IMIST.PRSM/morjchem-v12i2.46845

[35] O. M. H. Salo-Ahen, I. Alanko, R. Bhadane, A. M. J. J. Bonvin, R. V. Honorato, S. Hossain. Molecular dynamics simulations in drug discovery and pharmaceutical development. Processes. 9 (2020) 71.

[36] S. Bhaumik, A. Sarkar, S. Debnath, B. Debnath, R. Ghosh, M. E. Zaki, S. A. Al-Hussain. α-Glucosidase inhibitory potential of *Oroxylum indicum* using molecular docking, molecular dynamics, and in vitro evaluation, Saudi Pharm. J. 32(6) (2024) 102095.

[37] Y Y. Deswal, S. Asija, A. Dubey, L. Deswal, D. Kumar, D. Kumar Jindal, J. Devi. Cobalt(II), nickel(II), copper(II) and zinc(II) complexes of thiadiazole based Schiff base ligands: Synthesis, structural characterization, DFT, antidiabetic and molecular docking studies, J. Mol. Struct. 1253 (2022).

[38] O. M. Ogunyemi, G. A. Gyebi, A. Saheed, J. Paul, V. Nwaneri-Chidozie, O. Olorundare, J. Adebayo, M. Koketsu, N. Aljarba, S. Alkahtani, G. E. S. Batiha, C. O. Olaiya. Inhibition mechanism of alpha-amylase, a diabetes target, by a steroidal pregnane and pregnane glycosides derived from Gongronema latifolium Benth, Front. Mol. Biosci. 9 2022.

[39] P. Neupane, S. Dhital, N. Parajuli, T. Shrestha, S. Bharati, B. Maharjan, J. Adhikari Subin, R. L. S. Shrestha. Exploration of Anti-Diabetic Potential of *Rubus ellipticus* smith through Molecular Docking, Molecular Dynamics Simulation, and MMPBSA Calculation, J. Nepal Phys. Soc. 9 (2023) 95–105. DOI: https://doi.org/10.3126/jnphyssoc.v9i2.62410

[40] N. Lolok, S. A.Sumiwi, A. Muhtadi, Y. Susilawati, R. Hendriani, D. S. F. Ramadhan, J. Levita, I. Sahidin. Molecular docking and molecular dynamics studies of bioactive compounds contained in noni fruit (*Morinda citrifolia* L.) against human pancreatic α-amylase, J. Biomol. Struct. Dyn. 40 (2022) 7091–7098.

[41] R. L. S. Shrestha, B. Maharjan, T. Shrestha, B. P. Marasini, J. Adhikari Subin. Geometrical and thermodynamic stability of govaniadine scaffold adducts with dopamine receptor D1, Results Chem. 7 2024

[42] B. Xiong, Y. Wang, Y. Chen, S. Xing, Q. Liao, Y. Chen et al. Strategies for structural modification of small molecules to improve blood–brain barrier penetration: a recent perspective, J. Med. Chem. 64 (2021), 13152-13173.